

Permanent magnets for Faraday rotators inspired by the design of the magic sphere

G rard Tr nec,¹ William Volondat,¹ Orph e Cugat,² and Jacques Vigue^{1,*}

¹Laboratoire Collisions, Agr gats, R activit , UMR 5589, CNRS—Universit  de Toulouse, Universit  Paul Sabatier, Institut de Recherche sur les Systemes Atomiques et Moleculaires Complexes, F-31062 Toulouse, France

²Grenoble Electrical Engineering Laboratory (G2ELab), Institut Polytechnique de Grenoble—Universit  de Grenoble I—CNRS UMR 5269, BP 46; 38402 St Martin d'H res Cedex, France

*Corresponding author: jacques.vigue@irsamc.ups-tlse.fr

Received 23 March 2011; revised 22 June 2011; accepted 23 June 2011;
posted 14 July 2011 (Doc. ID 144642); published 16 August 2011

Faraday polarization rotators are commonly used in laser experiments. Most Faraday materials have a nonnegligible absorption, which is a limiting factor for high power laser optical isolators or for intracavity optical diodes. By using a stronger magnetic field and a shorter length of Faraday material, one can obtain the same polarization rotation and a reduced absorption. In this paper, we describe two permanent magnet arrangements that are easy to build and produce magnetic fields up to 1.7 T, substantially more than commonly used. The field homogeneity is largely sufficient for a 30 dB isolation ratio. We finally discuss the prospects for producing even larger fields with permanent magnets.   2011 Optical Society of America

OCIS codes: 230.2240, 140.0140.

1. Introduction

Following an original idea of Lord Rayleigh [1,2], optical isolators [3–7] are commonly used in laser experiments in order to prevent perturbations of the laser by light reflected by the setup. A closely related device is the optical diode, first described by Schr oder *et al.* [8], which is used to insure unidirectional oscillation in ring laser cavities (for more detail, see [9,10]). Both arrangements are based on the Faraday effect, i.e., the rotation of the polarization plane of a light beam induced by a magnetic field parallel to its propagation direction. The angle of rotation θ_F is given by

$$\theta_F = V \int B_z(z) dz \approx VB_0L. \quad (1)$$

Here, V is the Verdet constant and the approximate form assumes a constant magnetic field B_0 over the

length L of the Faraday material. Many efforts have been made to optimize optical isolators and diodes. The main problem comes from light absorption by the Faraday medium and this absorption reduces the transmitted power. The importance of this effect was recognized by Robinson [11], who introduced a figure of merit M for Faraday materials, defined by

$$M = \frac{V}{\alpha}. \quad (2)$$

In this equation, α is the absorbance defined by the transmitted intensity by a slab of material of thickness d , $I(d) = I(0) \exp(-\alpha d)$, where Fresnel reflection losses are not included.

Another consequence of light absorption is the distortion of the laser beam wavefront by the thermal lens effect. Because of the high power densities circulating in a laser cavity, the formation of a thermal lens in the Faraday material of the optical diode induces supplementary cavity losses, which limits the laser efficiency. Johnston and Proffitt [9] introduced another figure of merit M^* adapted to this case:

0003-6935/11/244788-10\$15.00/0
  2011 Optical Society of America

$$M^* = \frac{V}{\alpha} \times \frac{K}{(dn/dT)}, \quad (3)$$

where K is the thermal conductivity of the Faraday material and dn/dT is the derivative of its index of refraction with respect to temperature T . More recently, the same problem appeared in optical isolators that are used with high power cw lasers, as in the gravitational wave detectors (LIGO, VIRGO, etc.) [12,13]. A detailed analysis of the depolarization in the Faraday material due to thermally induced birefringence has been developed by Khazanov and co-workers [14–20] and these authors have demonstrated how to minimize this effect.

Various other efforts have been made to optimize these devices.

- The search for better Faraday materials. In the visible and near-infrared range, one of the best materials is terbium gallium garnet (TGG), which has a very large Verdet constant [21–23], $V_{633} \approx -134$ rad/(T·m) at $\lambda = 633$ nm, and a low absorbance $\alpha \approx 0.002$ cm⁻¹ in its transparency region [12,13]. Several other materials with a large Verdet constant have been recently studied [24–26]: their Verdet constant as well as their figure of merit M have been measured and some of them appear to be quite promising.

- TGG is a paramagnetic material and its Verdet constant increases rapidly when the temperature T decreases [27], almost like $1/T$. This property has led to the development of cryogenic Faraday rotators using TGG or TGG ceramic as the Faraday material [28–30].

A complementary technique to reduce the effects of light absorption by the Faraday material is to use a larger magnetic field B_0 and a shorter length L of Faraday material. Larger magnetic fields will be also very useful, either in the infrared region where TGG has a considerably smaller Verdet constant [21–23] (the Verdet constant decreases rapidly when the wavelength λ increases, in agreement with Becquerel equation [31], $V \propto \lambda \partial n / \partial \lambda$), or in spectral regions where one must use materials with a small Verdet constant or a rather large absorption (this is, for instance, the case in the 9 μ m wavelength range where the available Faraday material has an important absorption coefficient [32]).

To assign values, a Faraday isolator requires a rotation angle $\theta_F \approx 45^\circ$. At a wavelength $\lambda = 633$ nm, with TGG ($V_{633} \approx -134$ rad/(T·m)), $\theta_F \approx 45^\circ$ is obtained with $B_0 L \approx 6$ T·mm. The common magnet design [33] produces a magnetic field up to about $B_0 \approx 1$ T and the TGG rod length is $L \approx 6$ mm. By comparison, at $\lambda = 1064$ nm, $V_{1064} = -40$ rad/(T·m) at $\lambda = 1064$ nm and the rod length becomes $L \approx 20$ mm.

The goal of the current paper is to describe two magnet assemblies that are rather easy to build and provide a magnetic field B_0 up to 1.7 T and a field homogeneity largely sufficient for a good isolator. In

2008, a patent describing these two magnets was obtained by CNRS [34]. In 2009, Mukhin *et al.* [35] described a Faraday isolator with a 2.1 T magnetic field: the design of this magnet was similar to one of the designs described in the current paper. To produce this strong field, Mukhin *et al.* developed software able to predict the field created by a magnet assembly and they used this software to optimize their magnet on the following quantities: magnetic field value and homogeneity and weight of the magnet. Our work follows a completely different approach, based mostly on analytical calculations that explain how to produce a large magnetic field and what are the best arrangements; these calculations also provide scaling laws for the dependence of the field as a function of the magnet shape parameters. Finally, the isolation ratio of a Faraday isolator, which depends of the field homogeneity, has also been calculated. These theoretical predictions are in good agreement with the measurements done on the prototypes we have built. Finally, from our analytical results, we may estimate the maximum possible field and the magnet geometry needed to produce this field.

The paper is organized as follows. In Section 2, we describe the magic sphere of Zijlstra [36], which is the starting point of our work, and we calculate the field it produces at its center. In Section 3, we present two simpler designs based on the same principle and an analytic calculation of their main properties. In Section 4, we describe three prototypes we have built and the fields they produce. In Section 5, we discuss the limit on the isolation ratio due to the field inhomogeneity. In Section 6, we present some concluding remarks.

2. Magic Sphere

Hard ferromagnetic materials, such as samarium-cobalt (SmCo) or neodymium-iron-boron (NdFeB) compounds, have very strong magnetization and a very large coercive field. Moreover, these materials are very anisotropic so that their magnetization direction is almost fixed as long as they are not demagnetized. These properties make it possible to produce very strong magnetic fields with permanent magnets [37,38]. Several devices have been discussed, among which the magic sphere is the one of interest here.

A. Calculating the Magnetic Field of a Magic Sphere

This device, proposed by Zijlstra [36] in 1985, produces a large magnetic field at the coordinate origin O by using a distribution of magnetization in the surrounding space, with a density $\mathbf{M}(\mathbf{r})$. The contribution dB_z to the field at the origin due to the magnetization near any point \mathbf{r} is given by

$$dB_z = \frac{\mu_0 \mathbf{M}(\mathbf{r}) d^3 \mathbf{r}}{4\pi r^3} \times f(\theta, \psi), \quad \text{with}$$

$$f(\theta, \psi) = 2 \cos \theta \cos \psi + \sin \theta \sin \psi, \quad (4)$$

where θ is the polar angle. In order to maximize dB_z , $\mathbf{M}(\mathbf{r})$ is chosen in the meridian plane and ψ is the angle

between the vectors \mathbf{r} and \mathbf{M} (the angle between the z axis and \mathbf{M} is $\theta + \psi$). In the original design [36,39,40], $\psi = \theta$ and $f(\theta, \psi)$, thus, becomes a function of θ only, given by $f_z(\theta) = 1 + \cos^2 \theta$. If the magnetized material extends between two spheres of inner and outer radii r_i and r_e and if the magnetization modulus M is constant, the field at the origin O is given by

$$B_z(O) = \frac{4}{3} \mu_0 M \ln \left(\frac{r_e}{r_i} \right). \quad (5)$$

The field increases like the logarithm of the geometrical ratio r_e/r_i , and, as shown by Zijlstra [36], the field is homogeneous inside the internal sphere and vanishes outside the external sphere. Although the logarithm increases slowly, Eq. (5) predicts very large values of B_z with realistic values of the r_e/r_i ratio. $\mu_0 M$ is equal to the remanent field B_r of the magnetic material. In this paper, we will consider as an example NdFeB grades with B_r values in the range 1.2 – 1.45 T and, in all the numerical examples, we will use an intermediate value $B_r = 1.3$ T. With $r_e/r_i = 10$, Eq. (5) gives $B_z(O) = 3.07 B_r \approx 4$ T: this result is optimistic because some demagnetization will occur before reaching such a large field, but it is very encouraging.

A slightly better use of the magnetic material has been proposed by Bloch *et al.* [41–43]. The idea is to choose ψ as a function of θ so as to maximize the quantity $f(\theta, \psi)$ and the field $B_z(O)$, at the expense of its homogeneity. This maximum is obtained if ψ verifies $2 \tan \psi = \tan \theta$, which leads to $f(\theta)$ given by $f_{\text{BCTM}}(\theta) = \sqrt{1 + 3 \cos^2 \theta}$. The field $B_z(O)$ is then given by an equation similar to Eq. (5), with $4/3 \approx 1.333$ replaced by $\int_0^1 \sqrt{1 + 3x^2} dx \approx 1.380$.

B. First Constructions of Magic Spheres

It is practically impossible to produce magnets with a continuous variation of the magnetization direction so as to verify a continuous variation of ψ with θ , but it is possible to approximate this continuous variation by discretizing the structure into blocks of magnetic materials, each block having an homogeneous magnetization vector \mathbf{M} . The construction of magic spheres or cylinders with such blocks was patented in 1995 by Leupold and Tilak [44] and two approximations of the magic sphere have been built in the following way.

- In 1999, Bloch and co-workers [42,43] built an approximation of the magic sphere made of 12 meridian slices, each of them being built of 16 magnetic blocks. A 6 mm internal diameter polar bore was left free, without any material, and the external equatorial diameter of the magnetic material was 96 mm. This sphere produces a field $B_z \approx 2.5$ T, and up to $B_z \approx 5$ T if FeCo polar pieces are inserted in the polar bore, leaving a 150 μm gap.

- In 2000, Leupold and co-workers [39] developed a sphere producing a field $B_z \approx 1$ T in a 6.2 cm

long cavity for a traveling wave tube. The sphere external diameter was close to 18 cm and its mass was 22 kg.

These spheres are very complex to build with many magnet pieces of complicated shapes and, as NdFeB material is difficult to machine, their construction is long and very expensive. These difficulties explain why magic spheres have not been produced by industry. However, the idea that they could be very useful for optical isolators was already expressed by Leupold and Potenziani in their 1987 paper [40].

3. Simpler Designs Relying on the Same Principle

A. General Ideas

The idea of these designs is to keep the logarithmic increase of $B_z(O)$ with the ratio r_e/r_i but to use readily available magnets. In practice, it appears that only two directions of the magnetization $\mathbf{M}(\mathbf{r})$ are produced in rings: axial or radial. As in each case, both orientations are possible; we obtain four different relations between ψ and θ . These relations and the corresponding values of $f_i(\theta) = f(\theta, \psi)$ are listed below.

- Case 1: $\mathbf{M}(\mathbf{r})$ parallel to the Oz axis, i.e., $\psi = -\theta$ and $f_1(\theta) = 3 \cos^2 \theta - 1$.
- Case 2: $\mathbf{M}(\mathbf{r})$ antiparallel to the Oz axis, i.e., $\psi = \pi - \theta$ and $f_2(\theta) = -f_1(\theta)$.
- Case 3: $\mathbf{M}(\mathbf{r})$ radial outward, i.e., $\psi = \pi/2 - \theta$ and $f_3(\theta) = 3 \sin(2\theta)/2$.
- Case 4: $\mathbf{M}(\mathbf{r})$ radial inward, i.e., $\psi = \theta - \pi/2$ and $f_4(\theta) = -f_3(\theta)$.

Figure 1 presents a plot of the $f_i(\theta)$ functions as well as the optimum function $f_{\text{BCTM}}(\theta)$. We limit these plots and the discussion to the range $[0, \pi/2]$ because of symmetry when $\theta \rightarrow (\pi - \theta)$ (all equations are written with θ in radians, while numerical θ values are given in degrees).

The functions $f_1(\theta)$ and $f_2(\theta)$ are opposite and vanish for $\theta_{1,2}$, verifying $\cos \theta_{1,2} = 1/\sqrt{3}$, i.e., $\theta_{1,2} \approx 54.7^\circ$. The strong maximum in $\theta = 0$ is misleading: this region, which is weighted by $\sin \theta$ in integration, provides a minor contribution to the total field.

The function $f_3(\theta)$ corresponding to a radial outward magnetization is maximum for $\theta = 45^\circ$; this function nicely fills the gap between the regions where $f_1(\theta)$ or $f_2(\theta)$ is large. More precisely, $f_1 = f_3 = 1.28$ for $\theta_{1,3} = 29.3^\circ$ and $f_2 = f_3 = 0.78$ for $\theta_{2,3} = 74.3^\circ$.

B. Design of an “Axial-Only” Cylindrical Magnet

In this design (see Fig. 2), the magnetization \mathbf{M} is either parallel (for $0 < \theta < \theta_{1,2}$ and $\pi - \theta_{1,2} < \theta < \pi$) or antiparallel (for $\theta_{1,2} < \theta < \pi - \theta_{1,2}$) to the Oz axis. The contribution to B_z of the material near $\theta_{1,2}$, which is very weak, has the wrong sign when this border is crossed. An internal cylinder of radius r_i is kept free for the light beam and, rather than using an external sphere, the magnetic material extends up to a

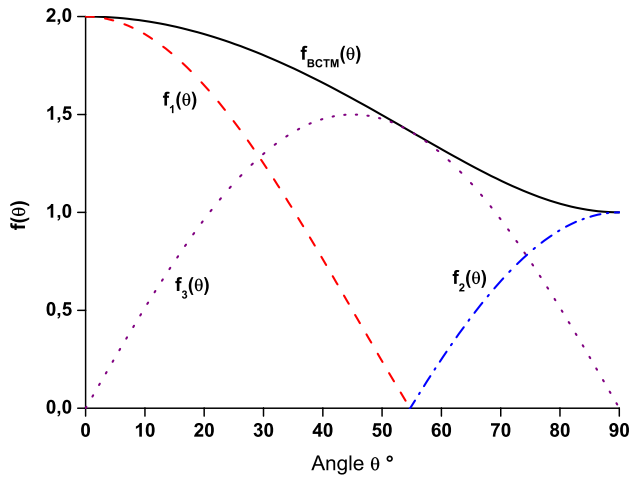


Fig. 1. (Color online) Plot of the functions $f_i(\theta)$ as a function of θ expressed in degrees. The solid black curve is the optimum function $f_{\text{BCTM}}(\theta) = \sqrt{1 + 3 \cos^2 \theta}$, while $f_1(\theta) = 3 \cos^2 \theta - 1$ is represented by the dashed red curve, $f_2(\theta) = -f_1(\theta)$ is represented by the dotted-dashed blue curve, and $f_3(\theta) = 3 \sin(2\theta)/2$ is represented by the dotted purple curve. We have plotted these functions only when they are positive and this explains why $f_4(\theta)$ does not appear in this figure.

cylinder of external radius r_e , which is not much more cumbersome in practice. For an infinite cylinder along the z direction, the field at the origin O is given by

$$B_{z,\infty}(O) = \frac{4}{3\sqrt{3}} B_r \ln\left(\frac{r_e}{r_i}\right) = 0.77 B_r \ln\left(\frac{r_e}{r_i}\right). \quad (6)$$

This result is similar to the magic sphere result [Eq. (5)], with the cylinder radii replacing the sphere radii and the coefficient 0.77 replacing the coefficient $4/3 \approx 1.33$. This substantially lower value is due to the very small contributions of the regions near $\theta_{1,2}$. The produced field may nevertheless be quite large:

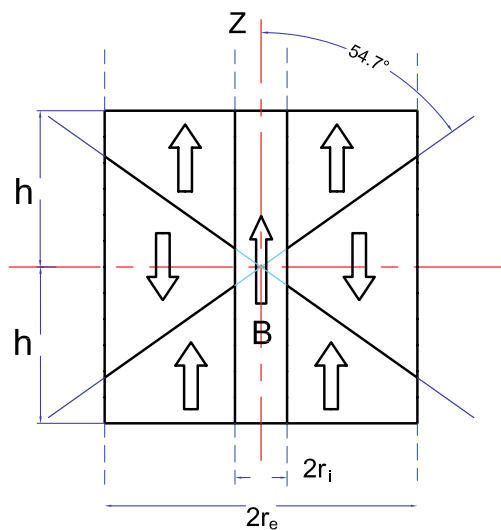


Fig. 2. (Color online) Meridian cut of an axial-only cylindrical magnet. The magnetized material extends between an internal cylinder of radius r_i and an external cylinder of radius r_e . The arrows indicate the magnetization vector \mathbf{M} .

with $r_e/r_i = 10$, Eq. (6) predicts $B_{z,\infty}(O) = 1.77 B_r \approx 2.3$ T. The assumption of an infinite cylinder along the z direction is not realistic. We can easily calculate the field of a finite cylinder extending from $z = -h$ to $+h$ if we assume that $h > r_e \tan \theta_{1,2}$, because, in this case, all the missing material would be magnetized along the z axis. The contribution to B_z of the missing material with $|z| > h$ is δB_z , given by

$$\delta B_z(O) \approx B_r \left[1 - \frac{1}{\sqrt{1 + (r_e/h)^2}} \right], \quad (7)$$

where a correction of the order of $(r_i/h)^2 \ll 1$ has been neglected. With $h = 1.5 r_e$, $\delta B_z = 0.17 B_r$ and the field produced by the truncated cylinder is given by $B_z(O) = B_{z,\infty}(O) - \delta B_z(O) \approx 1.60 B_r \approx 2.08$ T if $r_e/r_i = 10$.

It is important to evaluate the homogeneity of B_z near the origin O . We use the Taylor expansion of B_z up to second order and, thanks to cylindrical symmetry, to parity, i.e., $\mathbf{M}(-\mathbf{r}) = \mathbf{M}(\mathbf{r})$ and to $\nabla^2 \mathbf{B} = 0$, we get

$$B_z(x, y, z) = B_z(O) + B_{z,2} \frac{2z^2 - (x^2 + y^2)}{4}, \quad (8)$$

where $B_{z,2}$ is the second derivative of B_z with respect to z in O . $B_{z,2}$ is equal to

$$B_{z,2} \approx \frac{16 B_r}{9 \sqrt{3} r_i^2}, \quad (9)$$

where some minor terms have been neglected.

C. Design of an ‘‘Axial & Radial’’ Cylindrical Magnet

This design is represented in Fig. 3, with four orientations of the magnetization; each one being used where it is optimum. Here too, we assume that the magnetic material extends between two cylinders of radii r_i and r_e . For an infinite cylinder along the z direction, the field $B_{z,\infty}(O)$ is given by

$$B_{z,\infty}(O) = 1.23 B_r \ln\left(\frac{r_e}{r_i}\right). \quad (10)$$

This result is similar to the magic sphere result [Eq. (5)] and the coefficient $4/3 \approx 1.33$ is now replaced by 1.23. The loss with respect to the magic sphere is small and the field $B_{z,\infty}(O)$ may be very large. With $r_e/r_i = 10$, we get $B_{z,\infty} = 2.83 B_r \approx 3.7$ T if $B_r = 1.3$ T (as for the magic sphere, some demagnetization will reduce the predicted field). If we consider a finite cylinder extending from $-h$ to $+h$, we may use Eq. (7), provided that all the missing magnetized material is polarized parallel to the Oz axis, which requires that $h > r_e / \tan \theta_{1,3} \approx 1.78 r_e$. In conclusion, the axial & radial design is very efficient and produces a field close to the optimum represented by the magic sphere, but it is more complex to build than the axial-only design.

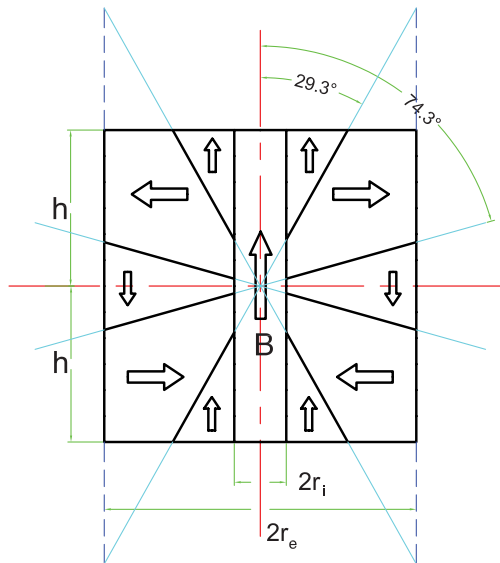


Fig. 3. (Color online) Meridian cut of an axial & radial cylindrical magnet. The magnetized material extends between an internal cylinder of radius r_i and an external cylinder of radius r_e . The arrows indicate the magnetization M .

D. Scaling Laws

Equations (6) and (7) for the axial-only cylindrical magnet or Eqs. (10) and (7) for the axial & radial cylindrical magnet prove that the field depends only on ratio of geometrical parameters; this means that two similar magnets with the same geometry and same magnetic material but different scales will produce the same magnetic field at their center and also everywhere if we use scaled coordinates. In particular, as shown by Eq. (9) for the axial-only cylindrical magnet (but the result is general), the second derivative of the field behaves as the size scale power -2 . These two remarks may be of some practical importance.

4. Construction of Structures Following these Two Designs

Magnetized rings of NdFeB are commonly produced with custom design and one may choose the material grade, with a trade-off between the remanent field B_r and the coercive field H_c . All the devices described here were built with NdFeB rings produced by the ChenYang company [45]. The manipulation of these rings requires great care because of the very large magnetic forces. A nonmagnetic central rod is used to guide these rings. Consecutive rings with the same direction of magnetization, which attract each other, are assembled first, and the assemblies thus produced, which repel each other, are compressed in an aluminum alloy box until they are in contact.

A. Prototypes of the Axial-Only Design

We have built two such prototypes made of a series of ring magnets and represented in Fig. 4. The ring dimensions being given in Table 1.

In prototype 1, our goal was to demonstrate the feasibility by producing a large field $B_z(O)$ at the cen-

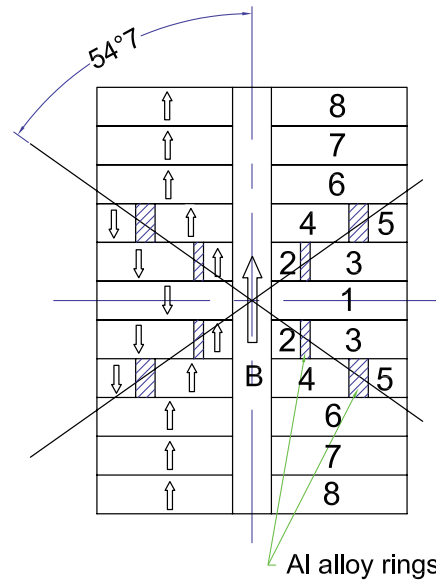


Fig. 4. (Color online) Drawing of our axial-only prototypes: magnetization is indicated by arrows. The ring dimensions are given in Table 1 for the two prototypes. Aluminum alloy rings are placed on the border line between opposite magnetization.

ter, without any other constraint. The cylinder radii are $r_i = 5$ mm and $r_e = 40$ mm and the total length is $2h = 110$ mm. In this prototype, the rings labeled 1–5 are of N42SH grade ($B_r = 1.35$ T, $H_c = 1.6$ MA/m) while rings 6–8 are of N50M grade ($B_r = 1.47$ T, $H_c = 0.88$ MA/m).

In prototype 2, our goal was to produce an optical diode for a Nd:YVO₄ ring laser emitting at 1342 nm: this laser is frequency doubled by an intracavity LiB₃O₅ crystal in order to produce 671 nm light (more details in [46]). When using intracavity frequency doubling, it is extremely important to

Table 1. Dimensions (in Millimeters) of the Rings Used for the Axial-Only Prototypes, Following the Design of Fig. 4

Prototype 1			
Ring Number	Internal Diameter	External Diameter	Thickness
1	10	80	10
2	10	25	10
3	30	80	10
4	10	50	10
5	60	80	10
6, 7, 8	10	80	10
Prototype 2 ^a			
Ring Number	Internal Diameter	External Diameter	Thickness
1	6.5	45	7.5
2	6.5	13	3.8
3	15	45	3.8
4	6.5	25	5
5	30	45	5
6, 7	6.5	45	7.5

^aThere are no rings number 8 in prototype 2.

minimize cavity losses and, in particular, absorption and beam distortion in the TGG crystal. We chose a TGG crystal length $L = 6$ mm in order to minimize absorption, and we have made a rough optimization of the magnet ring dimensions in order to maximize the field integral on the crystal length. The internal radius $r_i = 3.25$ mm was chosen large enough to insert a 6.35 mm diameter Hall probe used to measure the magnetic field, while the external radius $r_e = 22.5$ mm was limited by available space in the laser cavity. All the rings are made of N42SH grade.

Using a Hall effect probe, we have measured the magnetic field component B_z as a function of z for these two prototypes. The results are plotted in Fig. 5, as described below.

- For prototype 1, the field at the center of the cylinder is $B_z(O) = 1.72$ T and its second derivative extracted from the fit is $B_{z,2} = -0.057$ T/mm². These values are reasonably close to the predictions of Eqs. (6) and (7), which give $B_z(O) = 1.41B_r = 1.83$ T, and of Eq. (9), which gives $B_{z,2} = -0.053$ T/mm² (we used $B_r = 1.3$ T, although the grades used have a higher B_r value, to account for the small demagnetization due to the assembly). Finally, the integral $\int B_z dz$ over the central 6 mm is equal to 9.84 T·mm.

- For prototype 2, the field at the center of the cylinder is $B_z(O) = 1.49$ T and the integral $\int B_z dz$ over the central 6 mm is equal to 8.25 T·mm. These values are reasonably close to our numerical calculations, $B_z(O) = 1.59$ T and $\int B_z dz = 8.78$ T·mm. The predicted value of the second derivative [Eq. (9)], $B_{z,2} = -0.126$ T/mm², differs from the value extracted from the fit $B_{z,2} = -0.072$ T/mm², but, because of the optimization of the magnet ring

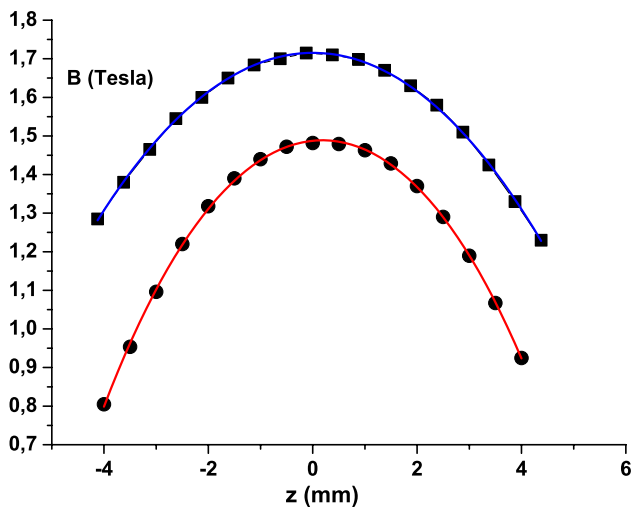


Fig. 5. (Color online) Magnetic field component B_z in Tesla measured as a function of z for our two prototypes following the two-orientation design: squares for prototype 1 and dots for prototype 2. In both cases, the data points are fitted by equation $B_z(z) = B_z(O) + B_{z,2}z^2/2 + B_{z,4}z^4/24$ (blue curve for prototype 1, red curve for prototype 2). The values of $B_z(O)$ and $B_{z,2}$ are discussed in the text; the contribution of the $B_{z,4}$ term is almost negligible.

dimensions, the design differs noticeably from the principle of Fig. 2 to which Eq. (9) applies.

B. Prototype of an Axial & Radial Design

We also built a prototype 3 inspired by the axial & radial design. In 2004, Brillet and Cleva [47] described to us the optical isolator used for the VIRGO experiment at that time and we designed this prototype with the same free diameter, $2r_i = 22$ mm. The disks with radial orientation are produced by assembling six triangular-shaped parts, with an homogeneous magnetization, in an external ring of aluminum alloy. Because these radially magnetized rings are expensive, we used only one type of such rings, with the two (inward or outward) directions of magnetization. This choice explains why our prototype strongly differs from the ideal arrangement of Fig. 3. In order to refine our design, we made simulations of the magnetic field using Flux2D software [48], assuming a perfect cylindrical symmetry.

The dimensions of this prototype are the following: internal radius $r_i = 11$ mm, external radius $r_e = 55$ mm, and total length $2h = 152$ mm (see Fig. 6). It is made of seven rings: three axial rings with their magnetization parallel or antiparallel to the z axis and four radial rings (two with inward magnetization and two with outward magnetization). The axial rings are 20 mm thick, with an external diameter 110 mm, and their material grade is N42SH ($B_r = 1.35$ T, $H_c = 1.6$ MA/m). The radial rings are 23 mm thick, with external diameter 90 mm for the magnetic material itself and 110 mm for the assembled ring inside an aluminum alloy ring, and their material grade is N50M ($B_r = 1.47$ T, $H_c = 0.88$ MA/m). Finally, the aluminum alloy box, not represented

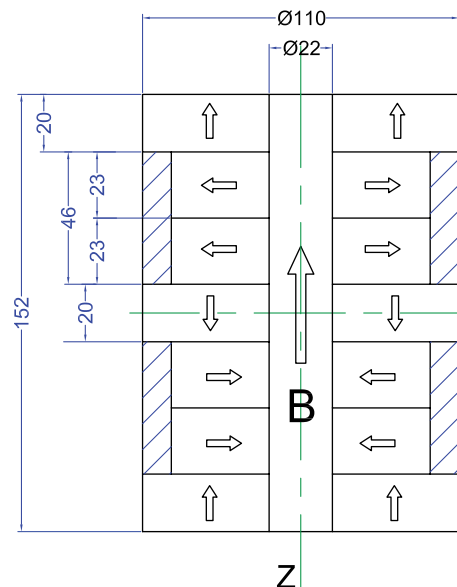


Fig. 6. (Color online) Drawing of our axial & radial prototype 3 (dimensions in millimeters). This magnet is made of three axial rings and of four radial rings (two with inward magnetization and two with outward magnetization). Magnetization is indicated by arrows.

in Fig. 6, has an external diameter of 130 mm and a total length of 172 mm.

Figure 7 presents a plot of the measured value of B_z in Tesla as a function of z . The maximum measured B_z value is $B_z(O) = 1.62$ T, while Flux2D simulation predicted $B_z(O) = 2.08$ T. We explain a part of this difference by the fact that the radially magnetized rings do not respect the cylindrical symmetry assumed in the simulation: they are made of six triangular parts of homogeneous magnetization and a calculation done by Bloch in his dissertation [43] shows that the on-axis magnetic field due to such a discretized ring is reduced by 17% with respect to a purely radial magnetization (we may note that this reduction factor would be only 5% for a ring made of 12 triangular parts instead of six). We also have an indication that some demagnetization occurred: immediately after the assembly, the maximum field measured was $B = 1.71$ T and this value decreased to 1.62 T a few days later, when the curve of Fig. 7 was recorded. This demagnetization is probably due to insufficient values of the coercivity and anisotropy of the central ring. Finally, the measured field decreases very slowly when going away from the center along the z axis, with $B_{z,2} = -0.0031$ T/mm², while Flux2D simulation predicted an opposite variation. We are not sure of the origin of this difference.

5. Requirements on the Field Homogeneity for Faraday Isolators

Many different effects [12,18,35,49] limit the performance of Faraday isolators. In this section, we discuss only the effect of the magnetic field inhomogeneity.

A. Theoretical Evaluation

To optimize a Faraday isolator, we must minimize the transmission of the return laser beam. If θ_F is

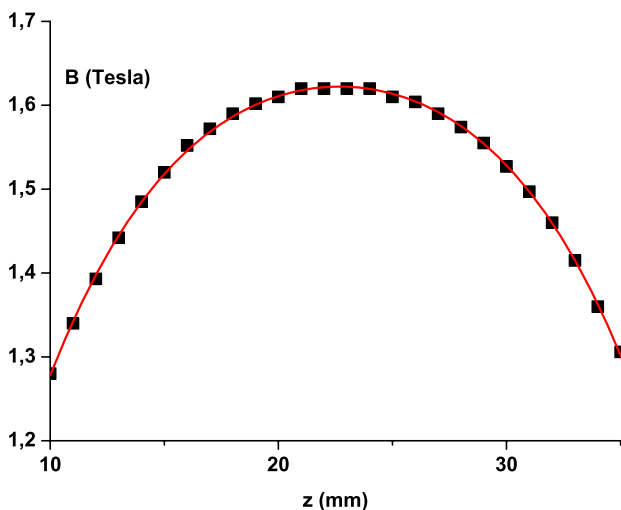


Fig. 7. (Color online) Magnetic field component B_z in Tesla measured as a function of z for our axial & radial prototype 3. The data points are fitted by an equation $B_z(z) = B_z(O) + B_{z,2}(z - z_c)^2/2 + B_{z,4}(z - z_c)^4/24$. The values of $B_z(O)$ and $B_{z,2}$ are discussed in the text; $B_{z,4}$ is almost negligible.

the Faraday rotation angle, the transmission T averaged over the light beam is given by

$$T = \int dS \frac{dP}{dS} \sin^2(\theta_F - \theta_0) / \int dS \frac{dP}{dS}. \quad (11)$$

Here, θ_0 is the angle defined by the entrance polarizer and dP/dS is the power density of the laser beam which will be assumed to be Gaussian and centered on the z axis. Then dP/dS is a function of the radius ρ :

$$\frac{dP}{dS} \propto \exp\left[-\frac{2\rho^2}{w^2}\right]. \quad (12)$$

$dS = 2\pi\rho d\rho$ and w is the local radius of the Gaussian beam (we neglect its variation over the length L of the Faraday material). In the calculations, the Gaussian beam extends only up to $\rho = pw$. The Faraday rotation angle θ_F is proportional to the integral $I(\rho) = \int B_z(z, \rho) dz$ over the Faraday material, which extends from $z = -L/2$ to $z = L/2$. We assume that Eq. (8) is sufficient to describe the variations of B_z and we get

$$I(\rho) \approx B_0 L + B_{z,2} \frac{(L^3 - 6\rho^2 L)}{24} \approx I_0 \left[1 - \frac{B_{z,2}}{4B_0} \rho^2\right]. \quad (13)$$

The $B_{z,2}L^3/24$ term can be omitted because it is small with respect to B_0L and independent of ρ . As $|\theta_F - \theta_0| \ll 1$, we replace the sine by its argument in Eq. (11). With the new variable $X = 2\rho^2/w^2$, the integrals are easy to calculate. The value of θ_0 is chosen such that it minimizes the transmission. This value is intermediate between the values of θ_F for $X = 0$ and for $X_{\max} = 2\rho^2$, and we note X_0 the value of X such that $\theta_F = \theta_0$. We get

$$T = \left[\frac{\theta_0 B_{z,2} w_0^2}{8B_0}\right]^2 \times \frac{X_0^2 K_0 - 2X_0 K_1 + K_2}{K_0} \quad \text{with} \quad (14)$$

$$K_n = \int_0^{X_{\max}} X^n \exp(-X) dX.$$

The minimum transmission, obtained for $X_0 = K_1/K_0$, is equal to

$$T_{\min} = \left[\frac{\theta_0 B_{z,2} w^2}{8B_0}\right]^2 \left(\frac{K_2}{K_0} - \frac{K_1^2}{K_0^2}\right) \approx \left[\frac{\theta_0 B_{z,2} w^2}{8B_0}\right]^2, \quad (15)$$

where the approximate value applies if $\exp(-X_{\max}) \ll 1$ (then $K_2 \approx 2$, $K_1 \approx K_0 \approx 1$).

B. Applications to Our Prototypes

Let us apply Eq. (15) to our prototypes. We assume that the Gaussian beam verifies $\rho_{\max} = 2.5w$ and we choose a ρ_{\max} value slightly smaller than the internal radius r_i of the magnet, to account for the support

Table 2. Values of $B_z(O)$, $B_{z,2}$, r_i , $\langle r_e \rangle$, and h , and the Chosen Value of ρ_{\max} for Each Prototype

Quantity	Prototype 1	Prototype 2	Prototype 3
$B_z(O)$ (T)	1.72	1.49	1.62
$B_{z,2}$ (T·m ⁻²)	-0.057	-0.072	-0.0031
r_i (mm)	5	3.25	11
$\langle r_e \rangle$ (mm)	40	22.5	49
h (mm)	55	27.5	76
ρ_{\max} (mm)	4	2.5	10
w (mm)	1.6	1.0	4
T_{\min} (dB) ^a	41	46	50
P ^b	0.94	0.91	0.74

^aThe calculated T_{\min} is given, expressed in decibels.

^bThe performance factor P is calculated using $B_r = 1.3$ T.

holding the Faraday rod. As usual, $\theta_0 \approx 45^\circ$. We have collected in Table 2 the relevant parameters and the calculated minimum transmission given by Eq. (15). We have also included a dimensionless performance factor P defined by the ratio of the measured value of the magnetic field at the origin O and of its theoretical value given by Eqs. (6) and (7) for an axial-only magnet and Eqs. (10) and (7) for an axial & radial magnet [in this second case, Eq. (7) is only an approximation because the length h is not large enough]. As in our prototype 3, the magnet external radius is not constant, and we use the mean value of this radius $\langle r_e \rangle$ in the equations. The performance factor P measures how close our prototypes follow the design of Figs. 2 and 3 and its values are discussed in Section 6.

Our axial-only prototypes produce a large field with a rather low homogeneity, which remains sufficient to provide an isolation ratio larger than 40 dB. The two prototypes achieve a field sufficient for a 45° Faraday rotation at $\lambda = 633$ nm with a short Faraday rod, with $L \approx 4$ mm. Prototype 3 provides a field with a very good homogeneity, and Eq. (15) predicts a 50 dB isolation ratio, even for a large beam with radius $w = 4$ mm. To achieve a 45° Faraday rotation at the wavelength $\lambda = 1064$ nm used in the gravitational wave detectors, the length of the TGG rod should be $L \approx 12$ mm. We were not able to test these predictions because we have no TGG rod with adequate length and antireflection coatings.

6. Concluding Remarks

In the current paper, we have shown that the magic sphere design can be modified to provide powerful magnets well adapted for high performance Faraday isolators as well as for intracavity optical diodes.

- The axial-only design is very easy to build and it already produces a maximum field larger than 1.7 T at the center of the structure, with a ratio $r_e/r_i = 8$. The achieved values of the performance factor P are larger than 0.9 for these two prototypes, thus proving the efficiency of this design. With this design, a field close to 2 T is feasible, by using a larger value of the r_e/r_i ratio. With this arrangement, the field decreases rather rapidly along the z axis away

from the center. The field homogeneity, which is not excellent, will limit the isolation ratio near 40 dB with the parameters of Table 2, but this value can be improved by reducing the laser beam radius with the same r_i value.

- The axial & radial design requires rings with radial magnetization, which makes this construction more costly, but we think that this design is very promising because it can provide a very strong field with an excellent homogeneity. As we had chosen a large internal radius $r_i = 11$ mm, we used a rather low value of the external radius $\langle r_e \rangle = 49$ mm, resulting in a rather low value of the maximum field, $B_z(O) = 1.62$ T. The performance factor is only equal to $P = 0.74$, and this is not surprising when one compares the theoretical and practical designs illustrated by Figs. 3 and 6. Obviously, we should be able to increase the field by following more closely the design of Fig. 3, by using radial rings made of eight or 12 parts rather than six, with an expected gain near 5% to 10%, and by increasing the r_e/r_i ratio.

- A similar axial & radial design was used by Mukhin and co-workers [35] who included ferromagnetic polar pieces and a ferromagnetic outer shield. The introduction of these ferromagnetic “conductors” produced a substantial gain on the magnetic field, with $B_z(O) = 1.7$ T increasing up to 2.1 T. We may also calculate the performance factor P for this magnet, using the parameters $r_i = 7.5$ mm, $\langle r_e \rangle = 66$ mm, and $h = 70$ mm. We have used $B_r = 1.2$ T because these authors state that $B_r = 1.2$ –1.3 T for most of the magnets and 1.0 T for the central axial magnet. We thus get a performance factor $P = 0.73$, similar to that achieved by our axial & radial prototype 3. The achieved field [35] is larger than that of our prototype 3, mostly because the $\langle r_e \rangle/r_i$ ratio is substantially larger for the magnet of Mukhin and co-workers than for our magnet, $\langle r_e \rangle/r_i = 8.8$ versus 4.5.

- The cost of these magnets is useful information. To build each prototype, we bought a quantity sufficient to build a few prototypes, with typically 10 units of each different ring. In this way, the cost of the magnets was about 400 USD for prototype 1, 200 USD for prototype 2, and 2000 USD for prototype 3.

Our results are still preliminary and a full optimization of these designs, based on detailed simulations, remains to be done. The largest possible field will ultimately be limited by demagnetization of the material near the center; several grades of NdFeB and of SmCo are able to withstand fields larger than 3 T, so that we may still expect large improvements.

We thank M. Büchner, M. Jacquey, and S. Lepoutre for their help, and A. Brillat and F. Cleva for interesting information. We acknowledge financial support from Centre National de la Recherche Scientifique (CNRS) Institut National de Physique (INP), Agence Nationale de la Recherche (ANR) (grant ANR-05-BLAN-0094), and Région Midi Pyrénées.

References

1. Lord Rayleigh, "On the constant of magnetic rotation of light in bisulphide of carbon," *Phil. Trans. R. Soc. London* **176**, 343–366 (1885).
2. Lord Rayleigh, "On the magnetic rotation of light and the second law of thermo-dynamics," *Nature* **64**, 577–578 (1901).
3. F. J. Sansalone, "Compact optical isolator," *Appl. Opt.* **10**, 2329–2331 (1971).
4. K. P. Birch, "A compact optical isolator," *Opt. Commun.* **43**, 79–84 (1982).
5. D. J. Gauthier, P. Narum, and R. W. Boyd, "Simple, compact, high-performance permanent magnet Faraday isolator," *Opt. Lett.* **11**, 623–625 (1986).
6. P. A. Schulz, "Wavelength independent Faraday isolator," *Appl. Opt.* **28**, 4458–4464 (1989).
7. R. Wynands, F. Diedrich, D. Meschede, and H. R. Telle, "A compact tunable 60 dB Faraday optical isolator," *Rev. Sci. Instrum.* **63**, 5586–5590 (1992).
8. H. W. Schröder, L. Stein, D. Frölich, B. Fugger, and H. Welling, "A high-power single-mode cw dye ring laser," *Appl. Phys.* **14**, 377–380 (1977).
9. T. F. Johnston and W. Proffitt, "Design and performance of a broad-band optical diode to enforce one-direction traveling-wave operation of a ring laser," *IEEE J. Quantum Electron.* **QE-16**, 483–488 (1980).
10. F. Biraben, "Efficacité des systèmes unidirectionnels utilisables dans les lasers en anneau," *Opt. Commun.* **29**, 353–356 (1979).
11. C. C. Robinson, "The Faraday rotation of diamagnetic glasses from 0.334 μm to 1.9 μm ," *Appl. Opt.* **3**, 1163–1166 (1964).
12. J. D. Mansell, J. Hennawi, E. K. Gustafson, M. M. Fejer, R. L. Byer, D. Cluble, S. Yoshida, and R. R. Reitze, *Appl. Opt.* **40**, 366–374 (2001).
13. The Virgo Collaboration, "In-vacuum optical isolation changes by heating in a Faraday isolator," *Appl. Opt.* **47**, 5853–5861 (2008).
14. E. Khazanov, "Compensation of thermally induced polarisation distortions in Faraday isolators," *Quantum Electron.* **29**, 59–64 (1999).
15. E. Khazanov, N. Andreev, A. Babin, A. Kiselev, O. Palashov, and D. H. Reitze, "Suppression of self-induced depolarization of high-power laser radiation in glass-based Faraday isolators," *J. Opt. Soc. Am. B* **17**, 99–102 (2000).
16. N. F. Andreev, O. V. Palashov, A. K. Potemkin, D. H. Reitze, A. M. Sergeev, and E. A. Khazanov, "A 45 dB Faraday isolator for 100 W average radiation power," *Quantum Electron.* **30**, 1107–1108 (2000).
17. E. A. Khazanov, "A new Faraday rotator for high average power lasers," *Quantum Electron.* **31**, 351–356 (2001).
18. E. Khazanov, N. Andreev, O. Palashov, A. Poteomkin, A. Sergeev, O. Mehl, and D. H. Reitze, "Effect of terbium gallium garnet crystal orientation on the isolation ratio of a Faraday isolator at high average power," *Appl. Opt.* **41**, 483–492 (2002).
19. E. Khazanov, A. Anastasiyev, N. Andreev, A. Voytovich, and O. Palashov, "Compensation of birefringence in active elements with a novel Faraday mirror operating at high average power," *Appl. Opt.* **41**, 2947–2954 (2002).
20. A. V. Voitovich, E. V. Katin, I. B. Mukhin, O. V. Palashov, and E. A. Khazanov, "Wide-aperture Faraday isolator for kilowatt average radiation powers," *Quantum Electron.* **37**, 471–474 (2007).
21. D. J. Dentz, R. C. Puttbach, and R. F. Belt, "Terbium gallium garnet for Faraday effect devices," *AIP Conf. Proc.* **18**, 954–958 (1974).
22. A. Balbin Villaverde, D. A. Donatti, and D. G. Bozini, "Terbium gallium garnet Verdet constant measurements with pulsed magnetic field," *J. Phys. C* **11**, L495–L498 (1978).
23. Terbium gallium garnet on Northrop Grumman website, <http://www.st.northropgrumman.com>.
24. W. Zhang, F. Guo, and J. Chen, "Growth and characterization of $\text{Tb}_3\text{Ga}_{5-x}\text{Al}_x\text{O}_{12}$," *J. Cryst. Growth* **306**, 195–199 (2007).
25. J. Liu, F. Guo, B. Zhao, N. Zhuang, Y. Chen, Z. Gao, and J. Chen, "Growth and magneto-optical properties of $\text{NaTb}(\text{WO}_4)_2$," *J. Cryst. Growth* **310**, 2613–2616 (2008).
26. F. Guo, J. Ru, H. Li, N. Zhuang, J. Liu, B. Zhao, and J. Chen, "Growth and magneto-optical properties of $\text{NaTb}(\text{MoO}_4)_2$ crystals," *J. Cryst. Growth* **310**, 4390–4393 (2008).
27. N. P. Barnes and L. B. Petway, "Variation of the Verdet constant with temperature of terbium gallium garnet," *J. Opt. Soc. Am. B* **9**, 1912–1915 (1992).
28. R. Yasuhara, S. Tokita, J. Kawanaka, T. Kawashima, H. Kan, H. Yagi, H. Nozawa, T. Yanagitani, Y. Fujimoto, H. Yoshida, and M. Nakatsuka, "Cryogenic temperature characteristics of Verdet constant on terbium gallium garnet ceramics," *Opt. Express* **15**, 11255–11261 (2007).
29. R. Yasuhara, S. Tokita, J. Kawanaka, T. Kawashima, H. Kan, H. Yagi, H. Nozawa, T. Yanagitani, Y. Fujimoto, H. Yoshida, and M. Nakatsuka, "Development of cryogenic TGG ceramic based Faraday rotator for inertial fusion driver," *J. Phys. Conf. Ser.* **112**, 032059 (2008).
30. D. S. Zhelezov, I. B. Mukhin, O. V. Palashov, E. A. Khazanov, and A. V. Voitovich, "Faraday rotators with short magneto-optical elements for 50 kW laser power," *IEEE J. Quantum Electron.* **43**, 451–457 (2007).
31. H. Becquerel, "Sur une interprétation applicable au phénomène de Faraday et au phénomène de Zeeman," *C. R. Acad. Sci.* **125**, 679–685 (1897).
32. L. Hilico, A. Douillet, J.-P. Karr, and E. Tournié, "Faraday optical isolator in the 9.2 μm range for QCL applications" (personal communication, 2011).
33. D. K. Wilson and A. Heiney, "Magnetic configuration for Faraday rotators," U.S. patent 4,856,878 (15 August 1987).
34. J. Vigué, G. Tréneç, O. Cugat, and W. Volondat, "Magnetic field generator having permanent magnets," Patent WO/2008/031935 A1 (30 March 2008).
35. I. Mukhin, A. Voitovich, O. Palashov, and E. Khazanov, "2.1 Tesla permanent-magnet Faraday isolator for subkilowatt average power lasers," *Opt. Commun.* **282**, 1969–1972 (2009).
36. H. Zijlstra, "Permanent magnet systems for NMR tomography," *Philips J. Res.* **40**, 259–288 (1985).
37. K. Halbach, "Design of permanent multipole magnets with oriented rare earth cobalt material," *Nucl. Instrum. Methods* **169**, 1–10 (1980).
38. K. Halbach, "Physical and optical properties of rare earth cobalt magnets," *Nucl. Instrum. Methods* **187**, 109–117 (1981).
39. H. A. Leupold, A. Tilak, and E. Potenziani II, "Permanent magnet spheres: design, construction and application," *J. Appl. Phys.* **87**, 4730–4734 (2000).
40. H. A. Leupold and E. Potenziani II, "Novel high-field permanent-magnet flux sources," *IEEE Trans. Magn.* **MAG-23**, 3628–3629 (1987).
41. F. Bloch, O. Cugat, G. Meunier, and J. C. Toussaint, "Innovating approaches to the generation of intense magnetic fields: design and optimization of a 4 Tesla permanent magnet flux source," *IEEE Trans. Magn.* **34**, 2465–2468 (1998).
42. F. Bloch, O. Cugat, J.-C. Toussaint, and G. Meunier, "Approches novatrices à la génération de champs magnétiques intenses: optimisation d'une source de flux à aimants permanents," *Eur. Phys. J. Appl. Phys.* **5**, 85–89 (1999).
43. F. Bloch, "Source de champ intense 4 Tesla aimants permanents," Ph.D. dissertation (Université de Grenoble, 1999).
44. H. A. Leupold and A. Tilak, "Field augmented permanent magnet structures," U.S. patent 5,428,334 (27 June 1995).
45. ChenYang Technologies GmbH & Co, <http://www.chenyang-ism.com/>.
46. U. Eismann, F. Gerbier, C. Canalias, G. Tréneç, J. Vigué, F. Chevy, and C. Salomon, "An all-solid-state laser source at

- 671 nm for cold atom experiments with lithium,” *Appl. Phys. B* (to be published).
47. A. Brillet and F. Cleva, ARTEMIS Observatoire Cote d’Azur, CNRS, Université de Nice Sophia Antipolis 06304 Nice (private communication, 2004).
48. Flux2D/3D, finite elements software package available from CEDRAT Company, www.cedrat.com.
49. J. Poirson, J.-C. Cotteverte, A. Le Floch, and F. Bretenaker, “Internal reflections of Gaussian beams in Faraday isolators,” *Appl. Opt.* **36**, 4123–4130 (1997).